Available online at www.sciencedirect.com

SCIENCE DIRECT®

Biochimica et Biophysica Acta 1656 (2004) 189–202

BIOCHIMICA ET BIOPHYSICA ACTA
BBA

www.bba-direct.com

# Quantum molecular dynamics simulation of proton transfer in cytochrome *c* oxidase

R.I. Cukier*

*Department of Chemistry, Michigan State University, East Lansing, MI 48824-1322, USA*

Received 27 October 2003; received in revised form 8 March 2004; accepted 11 March 2004

Available online 12 April 2004

**Abstract**

Proton transfer/translocation is studied in cytochrome *c* oxidase (CcO) by a combination of quantum mechanics (QM) for the transferring protons and classical molecular dynamics (MD) for the protein and solvent. The possibility of a glutamate, Glu286 in the *Rhodobacter sphaeroides* numbering scheme, acting as a rely point for proton translocation is investigated. The MD finds a hydrogen-bonded cycle of two waters and the carboxylate oxygens of Glu286. The possibility of protonating Glu286 to form neutral GluH is studied and we find that, as experimentally inferred, this glutamate can spend most of its time as GluH. Since translocation relies on the presence of water chains within CcO channels, MD is used to assess their formation. Glu286 and $Mg^{2+}$ can be connected by continuous hydrogen-bonded chains that are robust, though transient, and the protein appears spongy above (toward the outer membrane) the $Mg^{2+}$. In contrast, the D-channel spanning Asp132, close to the inner membrane surface, to Glu286, forms water chains that are much sparser and do not continuously connect these residues. Rather, there are chains spanning Glu286 to the vicinity of Asn140, and other more robust and ramified water structures that connect Asp132 with waters close to Asn140.


*Keywords:* Proton transfer and translocation; Cytochrome *c* oxidase

## 1. Introduction

Cytochrome *c* oxidase (CcO) is a membrane-bound enzyme that catalyzes the reduction of oxygen to water while producing an electrochemical gradient across the membrane in the form of a proton gradient. The mechanistic details of this process are quite complex, and many proposals for proton pumping have been developed [1–6]. These mechanisms involve proton transport through various channels containing waters that are hydrogen-bonded to each other and to residues. Proton translocation may occur via chains of hydrogen-bonded waters, using a "proton wire" concept [7] that has its origin in the Grotthuss [8] mechanism. The speed is attributed to an excess proton "hopping" along the water chain by a series of making and breaking hydrogen bonds, which does not require the slow process of molecular diffusion. The smallest version of a proton translocation chain is proton transfer between two waters or a water and a residue. Translocation and transfer rely essentially on the same phenomenon, the tunneling of proton(s) between heavy atoms as driven by the thermal fluctuations of the surroundings. CcO offers the possibility of many proton translocation/transfer events.

To describe proton translocation/transfer, it is desirable to use a quantum mechanical (QM) description of the proton(s) and a classical, molecular dynamics (MD) treatment of the other nuclear degrees of freedom. Therefore, we advance a methodology, previously termed the Adiabatic Simulation Method (ASM) [9–11], that combines a QM treatment of the transferring proton(s) with MD for updating the classically treated degrees of freedom, which is capable of describing the real-time dynamics of proton translocation/transfer in hydrogen-bonded chains, and apply it to CcO.

In this study, we focus on a region of CcO around a glutamate residue (Glu286) that has been suggested as critical to proton translocation [12–23]. This residue is found at the end of the so-called D-pathway [24–27] that, in *Rhodobacter sphaeroides*, stretches from Asp132, close to the inside (cytoplasmic side) of the bacterial membrane, to Glu286 that is between the *a* and $a_3$ hemes positioned deep within the protein. The MD assumes that Glu286 is

* Fax: +1-517-353-1793.
*E-mail address:* cukier@cem.msu.edu (R.I. Cukier).

0005-2728/$ - see front matter © 2004 Elsevier B.V. All rights reserved.
doi:10.1016/j.bbabio.2004.03.006

deprotonated, based on typical p$K_a$ values for a glutamate ( ~ 4.25) [28]. Whether an excess proton in the vicinity may protonate Glu286, with the aid of close-by water molecules, can shed light on the issue of the possible existence of a "glutamate trap" for protons [15,17].

To apply the ASM to proton translocation/transfer in CcO, hydrogen-bonded chains of waters and, possibly, residues must be found, and methods are developed to readily identify such chains. The MD simulation that we carry out shows that two water molecules become hydrogen-bonded to Glu286's carboxylate oxygens and that the waters are hydrogen-bonded to each other. This hydrogen-bonded "cyclic" structure of two waters and the carboxylate oxygens is quite persistent in time. Thus, once formed, a proton is added to one of the waters and the ASM method used to evaluate the possibility of proton transfer between the waters, and between one of the waters and one of the glutamate oxygens correlated with the water–water proton transfer. The protons do "hop" between their respective heavy atoms. The proton that is between a water and a carboxylate oxygen can spend comparable time hydrogen-bonded to the water and to the carboxylate, lending support to the experimental conclusion of a protonated Glu286.

Glu286 may be viewed as an essential point that connects the supply of protons from the D-pathway to ultimate proton exit on the outside of the membrane. Thus, we investigate the formation of water chains that can span the D-channel and water chains that span Glu286 to the $Mg^{2+}$ ion (referred to herein as the Mg-channel) that is present between Glu286 and the outside of the membrane. In our simulations we find that (1) there are robust water chains in the Mg-channel; (2) once waters are at the level of the $Mg^{2+}$, there are so many waters further above that the protein looks like a sponge in this region that should provide easy access to the outside; and (3) the D-channel is quite sparse, but does provide water chains, connected by a residue, suitable for translocation.

A number of informative simulations of CcO have been carried out before [29–34], which have addressed issues such as Glu286 acting as a proton shuttle [29,31], the formation of water chains [30,32,33,35] and the coupling between proton transfer and enzyme redox state [34,35]. Distinguishing features of our approach are the use of a quantum description of transferring protons, not enforcing any constraints on the positions of protein atoms, and the use of a large number of explicitly treated solvating waters [36].

## 2. Methods

### 2.1. Adiabatic simulation methodology

The ASM [9–11] uses a combination of quantum mechanics (QM) for the protons that can transfer, and MD for the heavy atom degrees of freedom. The Born–Oppenheimer separation between the fast proton motion and the slow heavy atom motion permits construction of proton potential surfaces parametric on the surrounding medium's (protein, heavy atoms in the hydrogen-bonded chain, cofactors) configuration. For a given potential surface, at a particular instant of time, we solve the Schrödinger equation to obtain the protons' wave function. With the protons' probability distributions (wave functions squared) and the conventional MD forces, the state of the system can be updated by an MD step. This new heavy-atom configuration provides a new potential surface for the protons, and the Schrödinger equation is solved again. If this scheme is iterated sufficiently, an account of proton transfer and translocation driven by medium thermal fluctuations can be given. A virtue of the ASM is the separation of the QM part for treating the protons from an almost conventional MD scheme for advancing in time the classical degrees of freedom, while still maintaining the "feedback" that the QM exerts on the MD and vice versa. A limitation of the ASM approach is that the quantum particle must be in a definite state. When the potential surface describing the proton's transit between the flanking heavy atoms, e.g. the two oxygens of a water dimer, has a low barrier for the transfer the proton ground state will dominate, satisfying the requirement of the ASM. In a protein environment, the heavy atom distances fluctuate. For large distances, the barrier is high and the transfer rate is very low. For short distances, the transfer rate is large, and these distances will be the most important to translocation/transfer. Thus, a good account of translocation/transfer can be obtained from the ASM.

Protons that will be treated quantum mechanically will be referred to as *active* protons. These protons are removed from the MD force field, because they will be treated quantum mechanically (as a wave function). In addition to the parameters defining the gas-phase potential energy surface that we obtain from high-level ab initio quantum chemical calculations on water clusters [37,38], van der Waals and charge parameters are required for their interactions with the surrounding atoms. Charge parameters, as a function of the proton's position, have also been evaluated by ab initio methods, though the precise values determined are method dependent [39]. The proton charge changes modestly as a function of position (from about 0.4 to 0.5 as the added proton transfers), and here we just assign it to be 0.45. The van der Waals oxygen parameters are set to those of the SPC water model used in the GROMOS [40] force field.

The atoms that are treated quantum mechanically will exert a force on each medium atom that has to be accounted for in the MD configuration update. The Hellmann–Feynman [41] theorem asserts that a quantum particle in a particular electronic state can be viewed as a classical charge distribution with density $|\psi(\mathbf{x}^n;\mathbf{R}^N(t))|^2$, obtained from the protons' wave function $\psi(\mathbf{x}^n;\mathbf{R}^N(t))$. Here, $\mathbf{x}^n$ denotes the coordinates of the $n$ quantum protons and $\mathbf{R}^N(t)$ those of the $N$ classical nuclei. These forces are obtained from the potential energy $V(\mathbf{x}^n;\mathbf{R}^N(t))$ that consists

of the sum of the gas-phase potential that must be obtained from an, e.g. ab initio calculation, and the solvation component that depends parametrically on the classical atom coordinates $\mathbf{R}^N(t)$. The time dependence arises from the MD trajectory that depends in a self-consistent manner on the forces generated from both classical and quantum degrees of freedom. Given a ground-state wave function $\psi(\mathbf{x}^N;\mathbf{R}^N(t))$, these forces can be obtained from the current MD configuration.

To solve for the protons' wave function, it is convenient to write the time-dependent Schrödinger equation in imaginary time since, from previous ASM work on electron localization in fluids, it is known that solution of the Schrödinger equation in imaginary time can be used to obtain ground states reliably and efficiently [9–11]. The wave function can be represented on a spatial grid and propagated by using fast Fourier transform methods [42,43].

### 2.2. Molecular dynamics

The MD simulation is carried out using CUKMODY, a code designed for the efficient simulation of proteins and other large solutes [44]. The GROMOS [40] force field is used for the residues and solvent water. The additions to the force field required to simulate CcO are discussed below. A combination of a cell index method with linked lists [45] and a Verlet neighbor list [46] is used to provide linear scaling with the number of atoms in the pair list routine, essential for the large systems considered here. For the Verlet neighbor list, the outer distance is $r_l = 12.8$ Å and the inner distance is $r_c = 10.0$ Å. The update of the pair list is done whenever any atom moves a distance greater than $0.5*(r_l - r_c)$, leading to updates roughly every 30 steps. The electrostatic interactions are evaluated using the charge-group method, to be consistent with the parameterization of the GROMOS force field. The SHAKE algorithm [46] is used to constrain bond lengths permitting a 2-fs time step. Periodic boundary conditions are used. The simulation is carried out at constant NVT, with velocity scaling to control the temperature to around 300 K. The start-up protocol creates a face-centered cubic (FCC) lattice of water molecules and centers the protein in the simulation cell. The waters that overlap the protein are discarded, based on their oxygen (atom O) to protein atom $j$ distance $r_{Oj} < \sigma_{Oj}$, with $\sigma_{Oj}$ the van der Waals distance parameter. The simulation is started with the protein cold, and the solvent heats the protein as the solvent molecules equilibrate to each other and the protein.

The starting configuration was obtained from a preliminary version [47] of the recently published X-ray crystal structure of CcO from *R. sphaeroides* [23]. Only subunits I and II were included in the simulation. The simulated protein had a total of 7,705 atoms, including the polar hydrogens that were added by use of the MOE program (Chemical Computing Group http://www.chemcomp.com/). After removing overlapping waters, there were 18,399 water molecules left in the simulation box. The simulation box side is 88.7 Å, and the largest dimension of CcO is around 80 Å, leaving about 20 Å between protein molecules in neighboring cells. The large number of waters used facilitates investigation of the formation of hydrogen-bonded water structures.

The histidine residues are assumed neutral (singly protonated), the aspartic and glutamic acids are ionized ($-1$), and the lysines and arginines are protonated ($+1$). A force field for the two heme *a*'s (with a farnesyl "tail") was constructed based on the GROMOS force field's heme *c*. Both heme groups are assumed to be in their reduced states, with formal charge $Fe^{+2}$. The $Cu_B$, assumed reduced ($+1$), is ligated to three histidine residues (His284, His333, His334). With charge delocalization to these histidines, the MD charge of $Cu_B$ is assigned as $+0.41$, a value essentially the same as used by Hofacker and Schulten [30]. The binuclear $Cu_A$–$Cu_A$ site forms a I–II mixed valence compound (Robin-Day type III) leading to formal charges of $+1.5$ per $Cu_A$ [48]. One $Cu_A$ is ligated to Glu254, Cys256, and His260, and the other to His217, Cys252 and Met264. For MD purposes, the charges are assigned as $+0.75$ per $Cu_A$, because of the charge transfer to the (deprotonated) cysteine ligands. The two His ligands are assigned $+0.25$ charge and each of the two (deprotonated) cysteine ligands a total charge of $-0.5$ [30]. The magnesium and calcium ions are assigned their formal charges of $+2$.

### 2.3. Water insertion and chain analysis

When waters are excluded by introducing the protein, as discussed above, approximately 12 are found inside the protein. (The number "inside" depends on a definition; we only consider waters that are within certain distances of the metals.) Because these lattice waters (LW) are from the initial FCC array, they most likely will not exhaust the interior room for waters. Therefore, we added additional interior waters by the following procedure. A van der Waals test sphere with water's $\sigma$ value is scanned over a grid with spacing of 1.5 Å in each of the three Cartesian coordinate directions. If the van der Waals interaction with neighboring atoms is less than 2 kcal/mol, this test sphere becomes a candidate test sphere. Each such candidate is then made into a test water (TW) by inserting water's electrostatic charges in the sphere. Each TW is "spun" over a set of 18 orientations, the energy evaluated for each orientation, and the minimum energy one accepted. Carrying this out for all candidates and accepting all whose energy lie below $-2$ kcal/mol provides a refined set of TWs. (Different choices for the energetic cutoffs lead to similar results, as long as the van der Waals energy is not chosen very large or the electrostatic very low.) Some of these waters are close to each other, because of the 1.5-Å grid spacing that we used. For those that are closer than a hydrogen-bonding distance (oxygen–oxygen distance less than 2.7 Å), one of the pair is eliminated. In this fashion, we finally have a set of TWs that

are incorporated in the MD simulation. For CcO, we include 500 such TWs. Of these, 5 (45) [228] are within a sphere of radius 10 (20) [30] Å that is centered on the protein's center of mass.

A program to construct hydrogen-bonded water "trees" was developed. While proton translocation is usually thought of in terms of proton "wires" or linear chains of hydrogen-bonded waters, the multi functionality of water and its donor/acceptor character leads, in principle, to tree versus chain structures. Of course, in the confinement of a protein, chain structures may dominate, and our procedure identifies them too. To construct a tree a "root" water is picked; for example, a water that we find hydrogen-bonded to Glu286. All waters (level 1) that are hydrogen-bonded to the root (level 0) are stored, and the root removed from the list of possible hydrogen bond formers. Each level 1 water is, in turn, considered as a root and all waters hydrogen-bonded to each of these are stored (level 2), and all level 1 waters removed from the list of possible hydrogen bond formers, and this procedure is continued recursively. Picking a desired number of levels, $N_{lev}$, will then produce, for all the MD steps considered, a tree of hydrogen-bonded waters of *at least* length $N_{lev}$. The criterion for hydrogen bond formation can be varied from, for example, "easy" where all members of a tree have Oa–Ob distance between the oxygens of waters a and b $d_{OaOb} < 3.5$ Å to "severe", $d_{OaOb} < 3.0$ Å and the OaHOb angle $A_{OaHOb}$ $180° < A_{OaHOb} < 145°$. Subsets of these trees can be selected by identifying a "terminator" atom. For example, if the Mg ion is picked as the terminator and Glu286 as the root, trees of all lengths of at least $N_{lev}$, spanning Glu286 to Mg will be selected. These trees are constructed every so often (we typically use 0.1 ps as an interval) to assess the statistics of chain formation/destruction.

## 3. Results

### 3.1. Formation of the Glu286 water cycle

MD simulation of the entire system—protein/cofactors, the 18,399 LWs and the 500 TWs—was initiated and carried out for more than 3 ns. On this time scale the overall protein structure is well maintained. The alpha-helical bundles that would span the membrane are persistent over the simulation with one exception. In the interface between subunits I and II, around Glu101 of subunit II, a possible K-pathway channel entrance [49], there is some loss of structure. This region is far from those that we analyze is in this work.

The MD trajectory was periodically examined for configurations of waters that are hydrogen-bonded together and to residues. Such clusters are tracked in time, with use of our tree algorithm, to find some that are relatively persistent. One such cluster that is spontaneously formed consists of two water molecules, a LW and a TW, and the residue Glu286. The two waters hydrogen-bond together, the LW hydrogen-bonds to the OE2 carboxylate oxygen, and the TW hydrogen-bonds to the OE1 carboxylate oxygen, as displayed in Fig. 1, at about 650 ps after startup. The alignment of the hydrogens, in their respective hydrogen bonds, is close to linear and the oxygen–oxygen atom distances are around 2.7 Å, indicating a strong hydrogen-bonding pattern. Examination of the dynamics of this cluster shows that it persists on the scale of hundreds of picoseconds, with the various heavy-atom, hydrogen-bonding distances undergoing small fluctuations. In the figure, we have replaced two hydrogens, one along the oxygen–oxygen line of centers and the other along the oxygen–OE1 glutamate oxygen, with ovals to denote that either one or both of these protons will be treated quantum mechanically, and added an extra proton to the water hydrogen-bonded to OE2. In view of the importance of Glu286 to mechanisms of proton transport in CcO, we will focus on this cycle with the ASM method.

### 3.2. Protonation of the Glu286 water cycle and single proton transfer

First, consider the possibility of single proton transfer between the two waters. An $H_5O_2^+$ molecule was formed by adding a proton to the LW that is directly hydrogen-bonded to OE2, as displayed in Fig. 1. The orientation of the added proton is defined by the geometry of the two waters. The potential energy surface for the active (quantum mechanical) proton can now be evaluated by moving the proton in its range between the two flanking oxygens and, for each proton position, evaluating the Coulomb interaction with the water, cofactor, and protein atom charges. The initial configuration (just after adding the excess proton) one-dimensional solvated proton surface for a heavy atom (oxygen1–oxygen2) distance $r_{12} = 2.7$ Å is displayed in Fig. 2A. Without solvation, the potential energy surface (for $H_5O_2^+$) is symmetric with a 5 kcal/mol barrier. Most of the solvation comes from the protein, though there are a number of relatively close-by waters that also contribute. The corresponding probability (wave function squared) is also displayed ( $\times 10$ for purposes of clarity). As discussed in Methods, this proton probability provides the Hellmann–Feynman forces on the surrounding atoms and these, along with the other MD forces, are used to advance the system's positions and velocities to the next MD configuration. The new configuration determines the new proton potential energy surface and the resulting forces, and the scheme is iterated. In Fig. 2B, we display the proton surface and probability 6 ps after the start of the ASM. Now the solvation has tipped the surface in favor of a transferred proton and the proton is localized on the other side of the double well.

A histogram of the solvation asymmetry (the energy difference between the right and left minima of the double well for each solvated state) is approximately Gaussian with

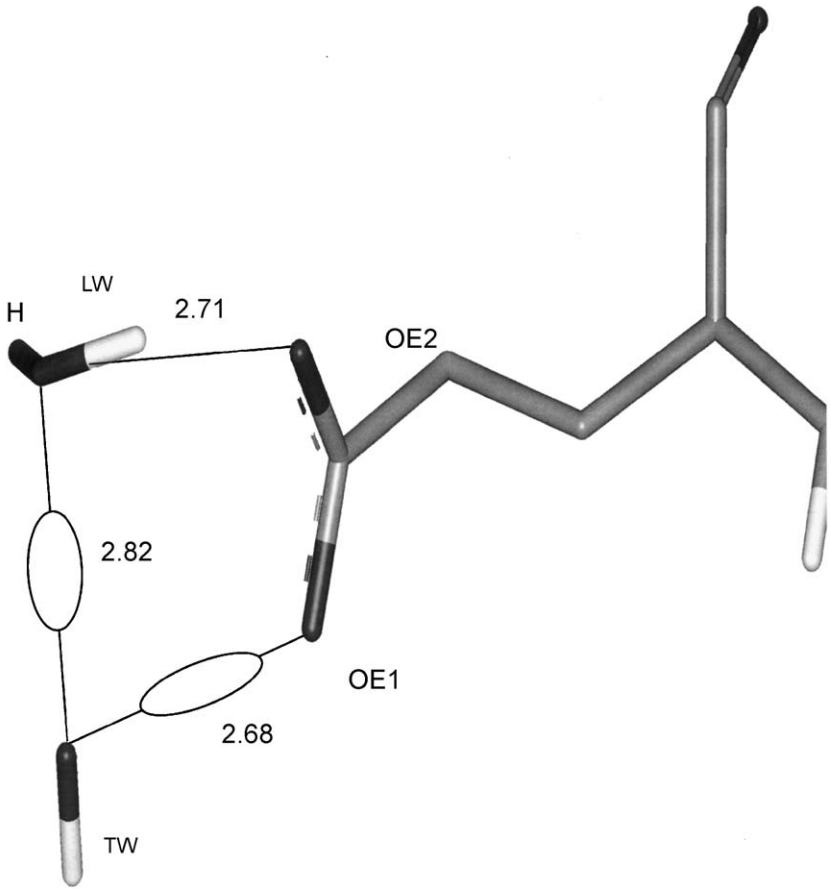


Fig. 1. The $H_5O_2^+$–Glu286 cycle consisting of two hydrogen-bonded waters that are hydrogen-bonded to, respectively, the OE1 and the OE2 of the carboxylate group of Glu286, with a proton added to the water hydrogen-bonded to OE2. The proton that forms the hydrogen bond between the two waters and the water proton that is hydrogen-bonded to OE1 are indicated as diffuse ovals, since they will be treated as wave functions in the two active proton ASM. The geometry indicates that all three hydrogen bonds are strong, and the structure is quite persistent in time. This configuration is used as the starting point for the ASM simulation.

a half-width at half-height of $\sim 4.1$ kcal/mol and a mean around 2.7 kcal/mol. The small mean value indicates that there is no strong asymmetry arising from the solvation. The solvation "bandwidth" of $\sim 4$ kcal/mol along with the fact that an asymmetry in the proton potential energy surface on a scale of $\sim 1$ kcal/mol is sufficient to essentially localize the proton on the lower energy side immediately suggests that a proton whose gas-phase potential energy surface is symmetric and does not have a very large barrier can oscillate between the two localized states on a fast time scale.

Fig. 3 displays the expectation value $\langle x\rangle(t)=\int dx\psi^*(\mathbf{x};\mathbf{R}^N(t))x\psi(\mathbf{x};\mathbf{R}^N(t))$ of the proton position versus time, after the waters and Glu have been equilibrated (several nanoseconds of MD). Data over only 20 ps are displayed for clarity of presentation, since it is typical of all the data. The proton clearly is quantum mechanically "hopping" back and forth between the two waters, and it does so on a several femtosecond time scale. The proton is mainly either left ($\langle x\rangle(t)\sim 1$ Å) or right ($\langle x\rangle(t)\sim 1.7$ Å) localized, depending on which way the solvation has tipped the proton potential energy surface (cf. Fig. 2).

### 3.3. Protonation of Glu286

Turning now to a two active-proton system that is of intense interest, as discussed in Introduction, consider the possibility of protonation of Glu286 by a hydrogen-bonded water molecule. To make this definite, consider the two waters and OE1 of Glu286 to form the proton chain, with the excess proton added to the LW (cf. Fig. 1). A potential surface for this system was obtained by quantum chemical methods, using the Gaussian 98 program package [50]. Accurate results can be obtained by use of the B3LYP density functional theory method with a 6-311 + G** basis set that includes polarization and diffuse functions on hydrogens and all heavy atoms, to describe the behavior of a proton or hydrogen atom. For this calculation [51], glutamic acid was replaced by acetic acid. The oxygen atom framework of the cluster was fixed close to the geometry from the simulation and the other atom coordinates were relaxed to obtain a stable geometry. The potential surface for the two active protons was generated by scanning their respective positions in 0.1-Å increments corresponding to transferring both protons. The configuration with the excess

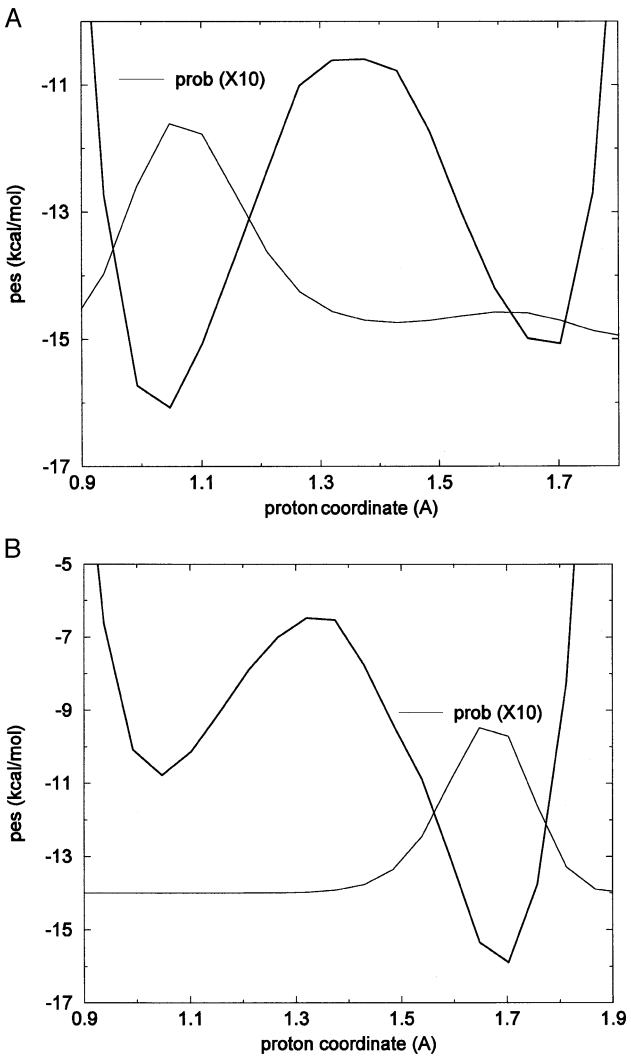


Fig. 2. (A) The initial state (after adding the excess proton) potential energy surface for moving the proton between the two waters (cf. Fig. 1), including the solvation component. The proton probability is displayed multiplied by 10 to show up on the scale of the potential energy surface. The solvation has tipped the potential energy surface in favor of the initial state by about 1 kcal/mol, and the proton is well localized on its initial state. (B) The potential surface 6 ps after the start of the ASM where solvation has tipped it in favor of proton localization in the final (proton-transfer) state.

proton transferred to the carboxylate, to form two waters and acetic acid, is more stable than the ionized form by about 35 kcal/mol. Thus, relative to a system with the carboxylic acid replaced by a water molecule, where the surface for the two active protons would be thermoneutral, the surface is quite strongly exoergic in favor of transferring a proton to the glutamate. The p$K_a$ of glutamic acid in protein environments is known, and tends to be elevated relative to its solution value [28,52]. Indeed, there is ample evidence for protonation of Glu286 at neutral pH, with an estimated p$K_a$ of 8 to greater than 9 [12,13,18,19,53]. Of course, there is a great difference between gas phase proton affinities and solution p$K_a$s. A p$K_a$ is a combination of local electronic structure energetic and solvation effects. In a

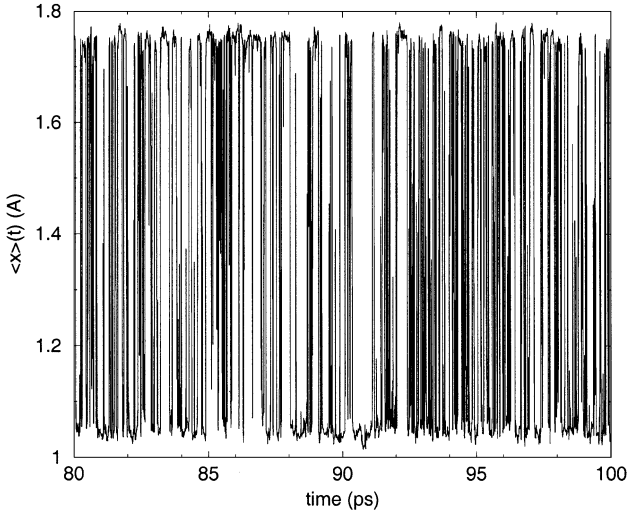


Fig. 3. The time-dependent expectation value, $\langle x\rangle(t)$, of the proton's position. Values around 1.0 Å (1.8 Å) indicate the proton is in its initial (transferred) state. The data for the interval between 80 and 100 ps are displayed, for clarity, from a run of 100 ps that was started after formation of the water–Glu286 cluster. The other data are similar in character.

protein the separation between local and solvation effects can be problematic, an issue elaborated in Discussion.

The two-active-proton species is then prepared for the ASM by protonating the LW, removing from the MD force field the hydrogen-bonded proton between the two waters and the hydrogen-bonded proton between the TW and the OE1. We then explore the dynamics of these two quantum protons for a series of asymmetries of the gas-phase potential.

Fig. 4 displays the expectation value of each proton's position over 100 ps after formation of the water Glu286 cluster, for $r_{12}=r_{23}=2.7$ Å, where the tendency to protonate

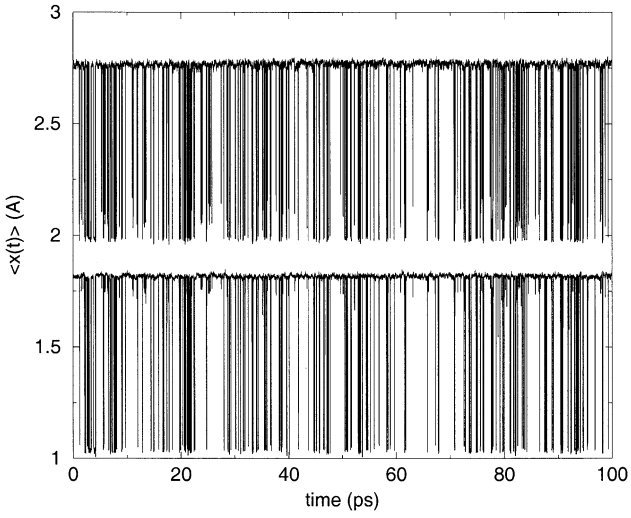


Fig. 4. The time-dependent expectation value $\langle x\rangle(t)$ of each proton's position. The second proton's gas-phase surface is exoergic by about − 9.25 kcal/mol in the direction of Glu286 protonation. The data for proton 2 are displaced by +1 Å for clarity of presentation. The jumps are highly correlated, reflecting the strong correlation induced by the ab initio surface.

the Glu is −9.25 kcal/mol exoergic. The second proton's expectation values $\langle x\rangle(t)$ are displaced vertically by 1 Å, for clarity of presentation. That is, proton 1 is covalently bonded to the LW (cf. Fig. 1) for $\langle x\rangle(t) \sim 1$ Å and covalently bonded to the TW for $\langle x\rangle(t) \sim 1.7$ Å and proton 2 is covalently bonded to the TW for $\langle x\rangle(t) \sim 2$ Å and covalently bonded to Glu for $\langle x\rangle(t) \sim 2.7$ Å (to form glutamic acid). Both protons do quantum mechanically transfer on a sub-picosecond time scale. The second proton transfers, indicating that Glu286 can be protonated by proton transfer from the water hydrogen-bonded to it. With this driving force to protonate the Glu, the second proton spends most of its time to form the carboxylic acid, GluH, and note that there is a strong correlation with the first proton's state. This follows from the nature of the typical ab initio surfaces that correlate the protons.

A free energy $\Delta G$ and corresponding equilibrium constant $K_{eq}$ for each proton can be obtained from the fraction of time each proton spends in its two states. This is an advantage of the QM treatment of the protons used here. The nature of this equilibrium constant will be addressed below. The experimental design [53] that infers high p$K_a$ values for Glu286 relies on the assumption of proton pre-equilibrium between the bulk and E286, which provides the bulk concentration of protons at the protein active site. Then, pH − p$K_a$ values can be inferred from the fraction of protonated Glu286 in the protein [53]. Under the same assumption, the simulation's ratio of protonated to deprotonated Glu286 populations can be used in the Henderson–Hasselbalch equation [54], pH − p$K_a$ = log[GluH]/[Glu$^-$], to infer a pH − p$K_a$ value. Table 1 summarizes the pH − p$K_a$s for various asymmetries that reflect the endo- or exoergic nature of the potential energy surface for the two-water and glutamate structure. If the TW–OE1 proton surface is −12 kcal/mol exoergic, this implies a p$K_a$ of 8.67 relative to a pH of 7. When there is no difference between a water and a glutamate in terms of the gas-phase surface, the first proton (the one between the two waters) spends essentially equal time in each state, so its $K_{eq} \approx 1$. For the second proton (the one between the TW and the OE1), $K_{eq} \approx 0.27$ leading to a $\Delta G \approx 0.7$ kcal/mol, a modestly endothermic protonation process.

Table 1
Proton transfer in the $2H_2O{\cdot}H{\cdot}$GLU286 cycle

| $\Delta E^{ab}$ | $K_{eq}(1)$ | $\Delta G(1)$ | $\Delta$pH(1)[c] | $K_{eq}(2)$ | $\Delta G(2)$ | $\Delta$pH(2) |
|---|---|---|---|---|---|---|
| 0.00 | 1.15 | −0.08 | −0.06 | 0.14 | 1.19 | 0.86 |
| 2.55 | 1.97 | −0.41 | −0.29 | 0.09 | 1.44 | 1.04 |
| 4.00 | 0.86 | 0.09 | 0.07 | 0.02 | 2.36 | 1.71 |
| −5.95 | 3.28 | −0.71 | 0.52 | 2.44 | −0.54 | −0.39 |
| −9.25 | 13.58 | −1.57 | −1.13 | 8.62 | −1.29 | −0.94 |
| −12.00 | 51.85 | −2.37 | −1.71 | 47.21 | −2.31 | −1.67 |

[a] All energies and free energies are given in kcal/mol.
[b] $\Delta E$ is the assumed endo ($\Delta E>0$) or exoergidicity ($\Delta E<0$) for protonation (by proton 2) of GLU286.
[c] $\Delta$pH ≡ pH − p$K_a$.

### 3.4. Hydrogen-bonded chains

The tree algorithm sketched in Methods can be used to examine the formation of various water trees in the protein. To examine the formation, breakup and persistence of such trees, water coordinates are written out every 0.1 ps. In order to make this scheme manageable, it proves convenient to focus on waters that correspond to various putative water channels that have been suggested as important to translocation in CcO and on channels that we have identified from preliminary simulations. Here, we will focus on two particular channels: (1) the D-channel that stretches from Asp132 (close to the inside membrane) to Glu286 and (2) a channel that we will refer to as the Mg channel that spans Glu286 to the region around the $Mg^{2+}$ ion. Because some protons reach Glu286 via the D-channel, and they may be responsible for protonating Glu286, which in turn can rely a proton to residues/waters that are continuing in an upward direction, it is interesting to also consider water chains that span Glu286 to the $Mg^{2+}$.

The waters that are considered for analysis are those found in cylinders with central axes defined by the two residues/ions of interest and a radius chosen to be 10 Å. One residue/ion of a cylinder is considered as an origin and we look for a "root" water that is hydrogen-bonded to this residue/ion. For the other residue/ion at the end of the cylinder, a terminator water is defined by its hydrogen bonding to this residue/ion. For example, in our Mg-channel, a water that is hydrogen-bonded to the Glu286 OE1 (OE2) is considered as a root and a water that is hydrogen-bonded to the $Mg^{2+}$ ion is considered as a terminator. Naturally, a root water may or may not persist for a "reasonable" time period. Somewhat arbitrarily, we define a root water as one that persists on a 100-ps time scale and similar for a terminator. Persistence for such times would permit ample time for translocation. Of course, the intervening waters between root and terminator are forming and breaking their hydrogen bonds. Thus, the chains are only in existence for a fraction of the persistence time of the root and terminator. In our counting of hydrogen bonds, we may use "easy" or "strict" criteria (see Methods); thus, the persistence of chains will depend on their definition.

### 3.5. Glu286–$Mg^{2+}$ channel

Once Glu286 is protonated, it may transfer this proton through chains of water molecules to deliver it to various residues/ions. Here, we will investigate the possibility of water pathways that stretch from Glu286 to $Mg^{2+}$, the Mg-channel. A snapshot from a MD time around 1.4 ns is displayed in Fig. 5. There are 13 waters in this chain and this is one of the longer ones that we have found in the 200 ps of data analyzed for this 1.4–1.6 ns time slice. The shortest chain has seven waters and the longest has 16. Thus, the chains can be quite convoluted. Furthermore, we have not displayed waters that are hydrogen-bonded to

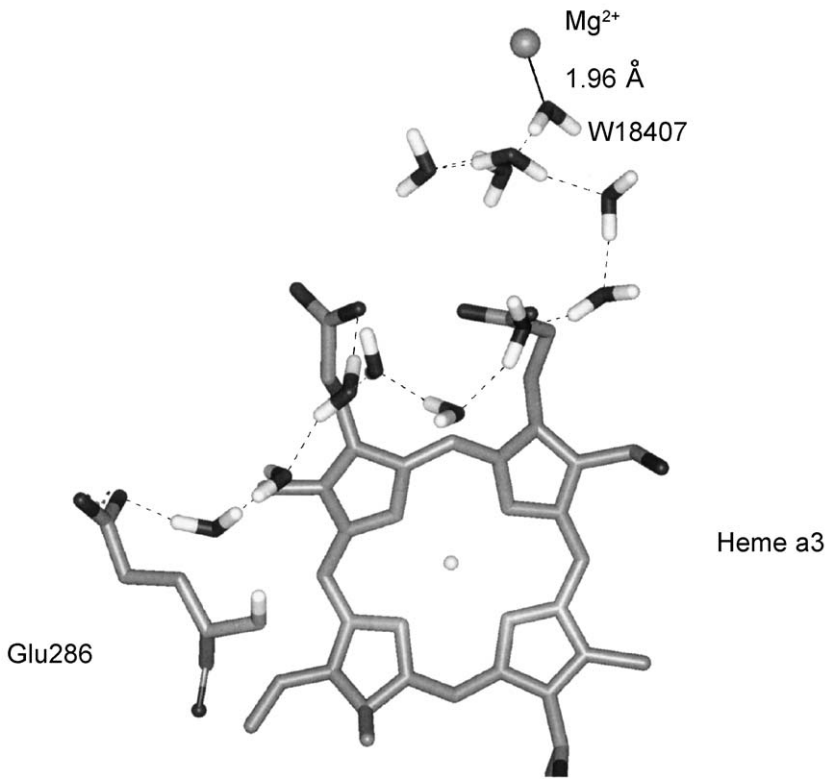


Fig. 5. A chain of hydrogen-bonded waters that have formed spanning Glu286 to $Mg^{2+}$. One end of the chain has a water hydrogen-bonded to the Glu286 carboxylate and the other end has a water ligated to $Mg^{2+}$. This snapshot is at a time around 1.4 ns after the beginning of the MD run. There are branches from the chain (not shown) of waters hydrogen-bonded to some of the displayed waters.

waters in the chain that spans from root to terminator. In the Mg-channel, as one proceeds from Glu286 toward the $Mg^{2+}$, the ramification of the tree increases, on average, indicating that the $Mg^{2+}$ end holds a greater water density than the glutamate end. For the strict definition of a hydrogen-bonded chain used here, and these particular root and terminator waters, spanning chains are present about 5% of the time. Using the easy criterion, these chains are present about 22% of the time. Thus, using any reasonable hydrogen bonding definition shows that there is ample opportunity to translocate an excess proton along such a hydrogen-bonded water chain.

### 3.6. Coordination of $Mg^{2+}$

That a terminator water, W18407, hydrogen-bonded to $Mg^{2+}$ is quite stable motivates examination of the ligand coordination of $Mg^{2+}$. The crystal structure indicates that there are three residues, His411, Glu254 and Asp412, and three waters associated with this ion; thus a six-coordinate structure. Whenever there are metals with coordinating ligands, there arises the issue of whether one should consider the metal–ligand interaction as non-bonded or bonded [55]. In a non-bonded model, there is the possibility of breaking coordination. Also, in a non-bonded model there will be a variety of coordination numbers since there is no directionality from orbital interactions. In our simulation, we have chosen a non-bonded model that essentially relies on electrostatics to maintain ligation. The simulation we carry out shows that, at least part of the time and for a relatively long time on the MD time scale (2 ns), the imidazole side chain of His411 breaks contact with the ion and moves $\sim 2-4$ Å away from it. However, the coordination is made up by a water replacing the His411 side chain. Also, the His411 Nε hydrogen-bonds to W18407. Fig. 6 shows this coordination pattern. Not surprisingly, the carboxylate residues' oxygens are symmetrically disposed with respect to the $Mg^{2+}$. If, as assumed, these residues are deprotonated, then the oxygens of the carboxylates are equivalent and will exhibit a strong tendency to be symmetrically disposed to an ion. A bonded model could enforce monodentate ligation of the carboxylates. Thus, the simulation may actually be indicating that the coordination should be stronger and it might require a covalent model of interaction with at least His411. Another possibility is that the loss of coordination with His411 may imply that it is deprotonated since, as is well established, residues ligated to positive ions can have the $pK_a$ of their ionizable sites substantially lowered [56]. If the histidine were an anion, its electrostatic interaction with $Mg^{2+}$ would be much stronger and would be much more likely to keep coordination with the cation.

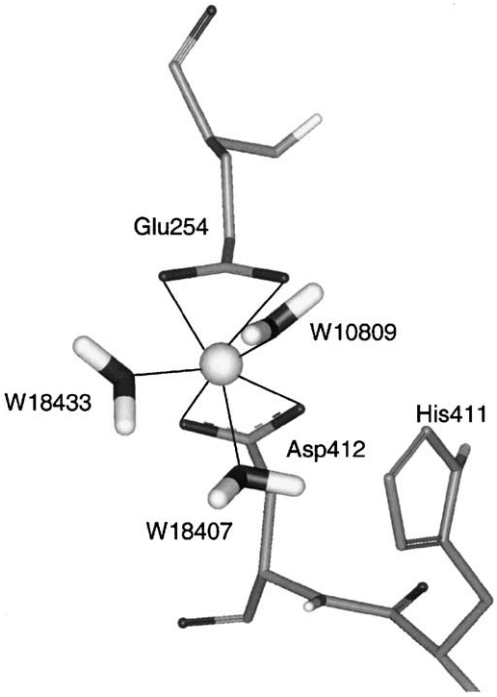


Fig. 6. Coordination sphere of $Mg^{2+}$ after 2 ns of MD. The carboxylates of Glu254 and Asp142 are symmetrically coordinated with the ion. The distances indicated with lines are all about 2.1 Å except for the $Mg^{2+}$ to W18407 distance that is 2.3 Å. The His411 imidazole has moved about 2 Å from its X-ray structure coordinates, its Nε hydrogen bonds to W18407, and a water has replaced it in the coordination sphere. Note that W18407, here part of the coordination sphere at 2 ns, is still present as part of the Mg-channel at 3 ns.

### 3.7. Glu286 conformational changes

There is experimental evidence [57], supported by a number of simulations [30,31], suggesting that Glu286 may undergo significant conformational changes in response to redox states of the protein. In our simulation, the enzyme is fully reduced—the only charge change we consider is protonation of Glu286. Fig. 7 displays the Glu286 orientation relative to the hemes at startup. Also displayed at the bottom in the same frame of reference is GluH286 (a) showing the orientation of the $Glu286^-$ after 650 ps of simulation with anionic Glu286, but drawn just after protonation. The Glu286 $COO^-$ flips up from an orientation that is relatively horizontal to a more vertical orientation, and the progression between these conformations occurs on a fast (tens of picosecond) time scale. Once the transition occurs, the GluH286 orientation is quite stable; it is approximately the same when the water cycle has formed around 650 ps and at 1 and 2 ns when the simulation is continued with (anionic) Glu286. In the beginning MD structure there is one water hydrogen-bonded to the carboxylate. At 650 ps there are two hydrogen-bonded waters, as displayed in Fig. 1. If, however, the Glu286 OE1 is protonated, as done at 650 ps, and the MD is then carried out with the now-formed GluH, there is another reorientation, denoted in Fig. 7 as GluH286 (b). This reorientation also occurs on a fast (tens of picosecond) time scale. Note that in going from $Glu^-$ to GluH, using the GROMOS force field, the charges on $COO^-$ are OE1 =OE2 = – 0.635 and CD = 0.27, while for COOH, the carboxylic acid, OE1 = – 0.548, OE2 = – 0.38, HE1 = 0.398 and CD = 0.53. Thus, it is not surprising that the change in charge distribution from $Glu^-$ to GluH can lead to a new conformation.

Not shown are the waters that are coordinated with $COO^-$ and COOH. The water cycle structures persist for long times and, so to speak, are dragged along with the rearranging side chain. Thus, the reorientation of Glu and GluH is intimately involved with the ability of this residue to create water chains that can translocate protons.

### 3.8. Glu286–Asp132 channel

The D-channel that stretches from Asp132 to Glu286 has been identified as an important source of vectorial and chemical protons [24–27]. Asp132 is close to a water pool and a number of histidine residues that may be implicated in providing sources of protons. The distance between Asp132 and Glu286 is greater than 30 Å and formation and persistence of a continuous, hydrogen-bonded water chain between these residues seems difficult to envisage. Of

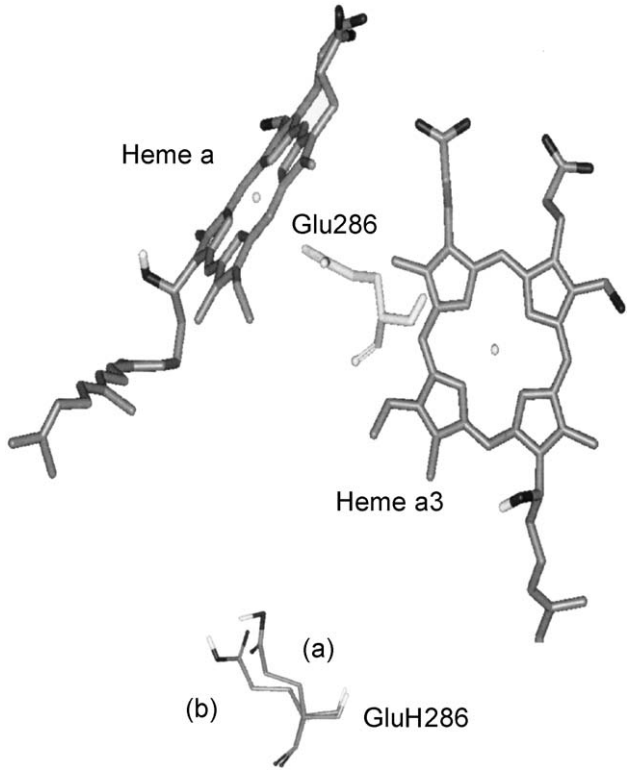


Fig. 7. The orientation of Glu286 relative to the two hemes for the starting, X-ray coordinates. The inner (outer) membrane is oriented downward (upward). (a) The orientation of GluH286 in the same frame of reference after 650 ps, when Glu286 has just been protonated and (b) 100 ps after this time. Two waters (not shown) are hydrogen-bonded to GluH at both times.

course, chains may also involve a number of residues, though examination of this region of the protein reveals it to be rather hydrophobic with some notable exceptions, in particular Asn139 and Asn140. That this is a rather hydrophobic region of the protein brings up the issue of the problem of populating the protein with waters by MD simulation, with its unavoidable short time scale. We find that there are roughly 20 waters in the D-channel at 200 ps, 40 at 1.5 ns and 60 at 3 ns. On this time scale the channel does appear to saturate as judged from the decreasing rate filling with time. Thus, introducing waters, even having used our TW method to find space in the protein and using a large number of solvent waters (see Methods), by MD may be problematic for establishing chains.

We were not able to identify continuous chains spanning Glu286–Asp132 even with the easy criterion for hydrogen bonding. However, there are hydrogen-bonded water trees that connect, for example, Glu286 to Asn140, as shown in Fig. 8. The tree extends about 25 Å from Glu286 to W517 whose oxygen is strongly and persistently hydrogen-bonded to the $NH_2$ group of this asparagine. Residues that are hydrogen bond donors (and those that are acceptors) can certainly participate in proton translocation. There is clearly an extensive hydrogen-bonded structure around Asp132.

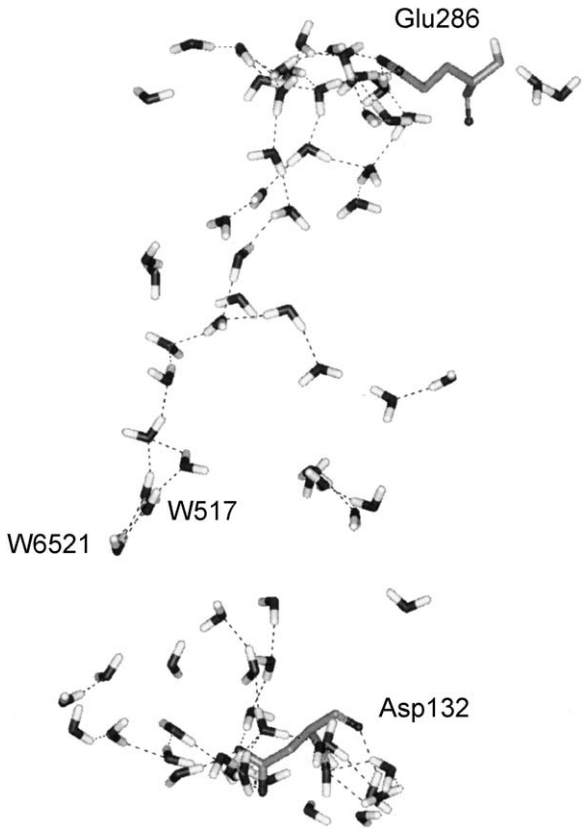


Fig. 8. A hydrogen-bonded tree spanning Glu286 OE2 to Asn140 that extends about 25 Å to W517. The structure is found by considering a water hydrogen-bonded to Glu286 OE2 as a root (W7475). The root water is present for about 40% of the (200 ps) interval examined here.

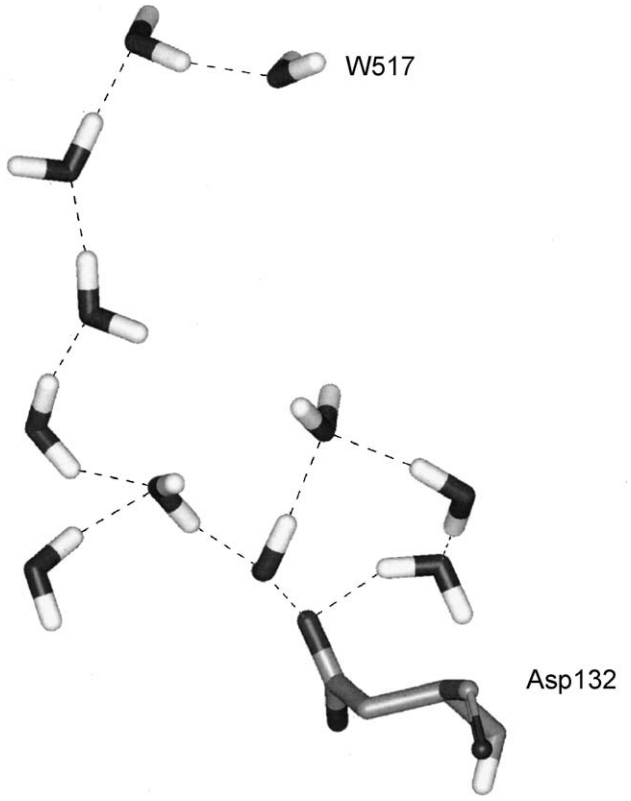


Fig. 9. A hydrogen-bonded tree of that spans W517 and Asp132's OD2. W517 is connected by a hydrogen-bonded pathway to Glu286 (see Fig. 8).

This kind of "network" is always present and indicates that Asp132 certainly is a good candidate for an entrance for protons. Note that our cylinder definition starts with Asp132's OE2, thus waters below this atom will not be considered as part of the network. Since this residue is so close to the solvent, there is no question that there is water pool available to provide waters. While not hydrogen-bonded continuously, some of the waters are quite close to W517. For example, W17884 is 5.7 Å from W517.

In investigating such structures, waters that are hydrogen-bonded to Glu286 were considered as root waters. For example, W7475 is hydrogen-bonded to Glu286 OE2 for about 40% of the 200-ps data examined here, and thus is a robust root water. In order to see if there are trees that connect W517 with Asp132, we consider W517 as the root and build trees toward Asp132. Treating W517 as the root leads to trees as illustrated in Fig. 9. There is a path leading to Asp132 and such structures are very robust. W517's oxygen is strongly hydrogen-bonded to Asn140's $NH_2$. Thus, the simulations are pointing to pathways that connect Asp132 and Glu286 with the intervention of a residue, Asn140.

## 4. Discussion

The MD simulation on CcO shows that quite rapidly (650 ps after initiation of the dynamics) two waters form

stable hydrogen bonds to Glu286, a residue that has been repeatedly implicated as contributing to proton translocation. The proton position expectation values for one active (quantum) proton or for two active protons, displayed in Figs. 3 and 4, support the notion of protonic "hopping" on a several-femtosecond time scale. Because it only takes on the order of a 1 kcal/mol asymmetry in the double well potential surface to localize a proton on the lower energy side (cf. Fig. 2), and because the solvent thermal fluctuations can produce a 1 kcal/mol asymmetry in a few (2 fs) MD time steps, the solvation contribution can switch which protonic state is stable on this time scale. This effect occurs even with the strong correlation between the two active protons induced by the gas phase potential surface. A mechanism of proton transport by classical mass diffusion would lead to a much slower dynamics.

Since it is based on a molecular description, the ASM method focuses attention on the connection between its predictions and experimental assessments of proton transfer and translocation. The solidity of this connection raises a number of issues that we now discuss. The protonation/deprotonation of Glu286's carboxylate oxygen leads to essentially equal proton population of the water and carboxyl oxygen when the gas-phase surface is assumed symmetric. By scanning over (assumed) asymmetry values, we have found that a few kcal/mol asymmetry leads to a substantial change in the protonation probability of Glu286. Because the solvation found here is essentially symmetric, it plays a minor role in prejudicing the obtained probabilities. Of course, the solvation bandwidth (around 4 kcal/mol in this simulation) is essential for producing these probabilities; without these fluctuations the protons would just stay in their respective initial states. We attribute the small solvation asymmetry to its essentially nonequilibrium character. For hydrogen-bonded structures that exist on a short (order 100 ps) time scale and for fast hopping between proton states, there is no opportunity to produce "equilibrium" solvation states that could have substantial asymmetry between initial and final proton states. Instead, the nonequilibrium, new proton state is eventually siphoned off to transfer the proton further along a chain of hydrogen-bonded waters and residues. Note, though, that we certainly cannot conclude that small solvation asymmetry is a generic feature. It is possible that specific charge interactions not included in the gas phase surface associated with particular residues could provide a substantial asymmetry, though in such a case it may be better to include these specific effects in the gas-phase potential. This is an issue for all calculations that divide the system into an "inner" part that is treated at a high level (usually some form of QM) and an "outer" part treated with a molecular mechanics force field. It should also be noted that when dealing with protonic wave functions (and probabilities) that have a finite width, the active protons appear to their surroundings as somewhat diffuse charge distributions, in contrast with the point charges used in classically based simulations. This effect will tend to decrease the difference in solvation from the different protonic states.

A utility of the ASM is the direct interrogation of the fractional protonated population. Because the fraction is obtained from a time average over the fluctuations in the surroundings, if the average can be carried out for a sufficiently long time to include many proton jumps, relating it to an equilibrium constant, a free energy and a p$K_a$ value has some operational utility. The direct connection between population and p$K_a$ does rely on the assumption of pre-equilibrium between the bulk and the E286 active site. That is, the rate of depopulation of the protonated glutamate, GluH, to lead to a protonated binuclear site, is slow compared to the supply of protons to $Glu^-$, as assumed in some of the experimental determinations of Glu286's p$K_a$ [53]. Even if these conditions are not satisfied, simulating the fractional populations is still useful. For example, if the $Glu^- + H^+ \rightleftharpoons$ GluH "equilibrium" can be experimentally probed over some time scale by, e.g. infrared spectroscopy, then from the differing frequencies of carboxylate versus carboxylic acid and the relative band intensities, the local populations can be inferred [12,13,16,18,19]. This population-based connection between simulation and experiment should be more direct than a relation to p$K_a$ values. Indeed, we assert that the fractional population is a more useful descriptor of the proton translocation process than p$K_a$ measurements.

Glu286 undergoes a two-stage rotation during the course of our simulations. Upon startup, there is a rapid (finished in about 100 ps) movement of the carboxylate side chain, relative to the crystal structure, to point higher up, in the orientation of Fig. 7. The crystal structure corresponds to the oxidized state of the enzyme, while the simulation assumes that the enzyme is fully reduced. Furthermore, in our startup, all the glutamates, including Glu286, are assumed to be unprotonated. Such differences could be responsible for the orientation change. Indeed, the crystal structure has one of the carboxylate oxygens of Glu286 within 2.6 Å of the carbonyl oxygen of Met107, suggesting the possibility that Glu286 is actually protonated in the oxidation state corresponding to the crystallographic data. Thus, it is not surprising that our simulation leads to a fast initial movement of Glu286. Upon protonation of Glu286, further MD of the neutral GluH286 rapidly leads to its carboxylate oxygens rotating by roughly 180° (see Fig. 7). This motion is accompanied by changes in the positions of the hydrogen-bonded waters associated with GluH286; the waters move to maintain their hydrogen bonding with GluH286. The motion of the Glu versus GluH and the association with hydrogen-bonded waters is qualitatively in accord with the findings of Pomès et al. [31] in their proposed proton shuttle mechanism and with a suggestion of Hofacker and Schulten [30]. Pomès et al. [31] used free energy methods to construct potentials of mean force for stable states of $Glu^-$ and GluH in association with "input and output" waters, and concluded that the stable states are separated by low

(1–2 kcal/mol) barriers, permitting facile conversion among them. The rapid and distinct changes in conformation found here are consistent with low barriers between the different conformations, and lend support to the proposed glutamate shuttle mechanism.

The role of Glu286 as a proton "trap" relies, of course, on its being supplied with and providing protons for proton translocation and transfer, for both chemical and vectorial protons. Our investigation of water trees in the D- and Mg-channels reveals an interesting contrast in behavior. The Mg-channel, stretching from Glu286 to the $Mg^{2+}$ ion, readily forms a great number of water trees that connect the residue and ion by a continuous and strong (recall the use of the strict criteria of oxygen–oxygen distance less than 3 Å and hydrogen bond angle deviation from linearity of no more than 35°) hydrogen-bonded chain. These pathways form relatively early in the MD, being in evidence robustly around 1 ns and increasing, on average, in tree size and persistence as the MD trajectory continuous toward 3 ns. Note that in the snapshot for Fig. 5, there are waters hydrogen-bonded to residues such as Arg481 and Arg482 (not displayed for clarity) and that a water (W18618) persistently hydrogen-bonds to the heme a3 D propionate; both features are seen in the crystal structure [23]. This latter pattern, along with hydrogen bonding to the heme a3 A propionate, is common in our simulations, lending support to the involvement of propionates for both chemical and vectorial protons. Once waters are around the $Mg^{2+}$, examination of snapshots from the MD trajectory shows that above this level the protein begins to look like a sponge. Indeed, the water tree algorithm in this region produces trees that begin to resemble the coordination associated more with bulk water than the interior of a protein. Thus, in our view, once protons have been translocated to the vicinity of $Mg^{2+}$, they should have no trouble exiting to the outside membrane surface. The MD-generated configurations just discussed refer to simulations with the glutamate not protonated. Examination of the protonated glutamate data leads to the same general conclusions. The simulations of Medvedev et al. [32] and Zheng et al. [33] on bovine heart CcO that use very different methods find similar water structures around the glutamate and $Mg^{2+}$ sites.

The D-channel water population is much sparser, requiring times around 3 ns before there is much evidence for sufficient water in the channel to investigate the occurrence of long chains. Indeed, even with the easy criterion of oxygen–oxygen distance less than 3.5 Å, no continuous chain connecting Glu286 and Asp132 was found. Of course, the D-channel spans more than 30 Å from Glu286 OE2 to Asp132 OD2, and this is much longer than the approximately 17 Å between the OE2 of Glu286 and the $Mg^{2+}$ of the Mg-channel. What is found are trees that connect Glu286 with Asn140, a distance of about 25 Å, and a ramified structure of hydrogen-bonded waters stretching about 10 Å from Asp132 to a water that is hydrogen-bonded to Asn140 (see Figs. 8 and 9). Thus, the simulations suggest that the D-channel can supply protons to Glu286 by two water structures that are connected around Asn140. Our results are in good qualitative agreement with the crystallographic data [23]. In the *R. sphaeroides* structure the residues in the D-pathway are defined as Asp132–Asn121–Asn139–Asn207–Ser142–Tyr33–Ser201–Ser200–Ser197–Glu286. We find, at this instant, that the following residues are hydrogen-bonded to waters: Asn121 W7443* and W1485, Asn139 W13501*, Asn207 W5575, Tyr33 W1485, Ser201 W18603, Ser200 W2146*, and Ser197 W18478* and W18484*, where * denotes waters that are part of the chain displayed in Fig. 8.

A number of approximations and restrictions in the work presented here should be noted. The separation of system into a quantum and a classical region is a seminal problem in all simulations that involve proton transfer/translocation and, more generally, bond making and breaking. Providing reasonable potential surfaces from quantum chemical calculations always implies an assessment of which residues should be included in the "gas phase" potential. The ASM simulation considered the oxygen–oxygen distances in the two waters–Glu286 cycle to be fixed. In a protein, these distances will fluctuate indicating that a vibrational force field for the oxygen–oxygen distances should be used. Because we find that our results are only modestly dependent on these distances, introduction of these effects should not lead to substantial modification of the results. However, the motion of the waters after protonation is an important issue to address. The addition of the excess proton and the switch from the MD force field to the quantum treatment of the active protons change the forces and may well lead to the cycle breaking up, or having additional water molecules. Indeed, in order for proton translocation to proceed, such events most likely must occur. Clearly, protonation of a water/residue cycle, or other structures that form, must lead to new geometric configurations that can pass protons across the membrane. We have not addressed by quantum/classical methods, such as the ASM, proton translocation along long chains since straightforward approaches to solving the Schrödinger equation scale with the number of active (quantum) protons to a power related to the number of basis functions used (or size of the Fourier basis). We have developed methods that should permit a scaling linear in the number of basis functions that could be applied in realistic computational times to three and more active protons even in computationally demanding systems as well-solvated CcO. Solvating CcO with exterior waters and by populating its interior with added waters relies on the slow (on an MD time scale) process of "diffusion" to produce water trees and chains. For channels that are difficult to populate on an MD time scale, other methods, based on, for example, biasing potentials that are used in free energy simulations, may have to be developed. Finally, in CcO the proton translocation process is induced by and coupled to the electron transfer events. Thus, a complete simulation will require investigation of different oxidation

states of the redox-active metals and their influence on the proton dynamics.

## Acknowledgements

The financial support of the National Institutes of Health (GM 47274) is gratefully acknowledged.

## References

[1] M.K.F. Wikström, Proton pump coupled to cytochrome *c* oxidase in mitochondria, Nature 266 (1977) 271–273.
[2] B.G. Malmström, Cytochrome *c* oxidase as a redox-linked proton pump, Chem. Rev. 90 (1990) 1247–1260.
[3] B.G. Malmström, Vectorial chemistry in bioenergetics: cytochrome *c* oxidase as a redox-linked proton pump, Acc. Chem. Res. 26 (1993) 332.
[4] S. Papa, N. Capitanio, G. Villani, G. Capitanio, A. Bizzoca, L.L. Palese, V. Carlino, E. De Nitto, Cooperative coupling and role of heme alpha in the proton pump of heme-copper oxidases, Biochimie 80 (1998) 821–836.
[5] S. Ferguson-Miller, G.T. Babcock, Heme/copper terminal oxidases, Chem. Rev. 96 (1996) 2889.
[6] See articles on cytochrome *c* oxidase in Biochemica et Biophysica Acta 1458 (2000).
[7] J.F. Nagle, S. Tristam-Nagle, Hydrogen bonded chain mechanisms for proton conduction and proton pumping, J. Membr. Biol. 74 (1983) 1–14.
[8] N. Agmon, The Grotthuss mechanism, Chem. Phys. Lett. 244 (1995) 456–462.
[9] A. Selloni, P. Carnevali, R. Car, M. Parrinello, Localization, hopping, and diffusion of electrons in molten salts, Phys. Rev. Lett. 59 (1987) 823–826.
[10] R.N. Barnett, U. Landman, A. Nitzan, Dynamics and spectra of a solvated electron in water clusters, J. Chem. Phys. 89 (1988) 2242–2256.
[11] J. Zhu, R.I. Cukier, A quantum molecular dynamics simulation of an excess electron in methanol, J. Chem. Phys. 98 (1993) 5679–5693.
[12] P. Hellwig, B. Rost, U. Kaiser, C. Ostermeier, H. Michel, W. Mantele, Carboxyl group protonation upon reduction of the *Paracoccus denitrificans* cytochrome *c* oxidase: direct evidence by FTIR spectroscopy, FEBS Lett. 385 (1996) 53–57.
[13] A. Puustinen, J.A. Bailey, R.B. Dyer, S.L. Mecklenburg, M. Wikstrom, W.H. Woodruff, Fourier transform infrared evidence for connectivity between CuB and glutamic acid 286 in cytochrome $bo_3$ from *Escherichia coli*, Biochemistry 36 (1997) 13195–13200.
[14] P. Adelroth, M. Svensson-Ek, D.M. Mitchell, R.B. Gennis, P. Brzezinski, Glutamate 286 in cytochrome $aa_3$ from *Rhodobacter sphaeroides* is involved in proton uptake during the reaction of the fully reduced enzyme with dioxygen, Biochemistry 36 (1997) 13824–13829.
[15] B. Meunier, C. Ortwein, U. Brandt, P.R. Rich, Effects of mutation of residue 167 on redox-linked protonation processes in yeast cytochrome *c* oxidase, Biochem. J. 330 (1998) 1197–1200.
[16] B. Rost, J. Behr, P. Hellwig, O.M.H. Richter, B. Ludwig, H. Michel, W. Mantele, Time-resolved FT-IR studies on the CO adduct of *Paracoccus denitrificans* cytochrome *c* oxidase: comparison of the fully reduced and the mixed valence form, Biochemistry 38 (1999) 7565–7571.
[17] S. Junemann, B. Meunier, N. Fisher, P.R. Rich, Effects of mutation of the conserved glutamic acid-286 in subunit I of cytochrome *c* oxidase from *Rhodobacter sphaeroides*, Biochemistry 38 (1999) 5248–5255.
[18] P.R. Rich, J. Breton, S. Junemann, P. Heathcote, Protonation reactions in relation to the coupling mechanism of bovine cytochrome *c* oxidase, Biochim. Biophys. Acta, Bioenerg. 1459 (2000) 475–480.
[19] D. Heitbrink, H. Sigurdson, C. Bolwien, P. Brzezinski, J. Heberle, Transient binding of CO to Cu-B in cytochrome *c* oxidase is dynamically linked to structural changes around a carboxyl group: a time-resolved step-scan Fourier transform infrared investigation, Biophys. J. 82 (2002) 1–10.
[20] C. Backgren, G. Hummer, M. Wikstrom, A. Puustinen, Proton translocation by cytochrome *c* oxidase can take place without the conserved glutamic acid in subunit I, Biochemistry 39 (2000) 7863–7867.
[21] A. Aagaard, G. Gilderson, D.A. Mills, S. Ferguson-Miller, P. Brzezinski, Redesign of the proton-pumping machinery of cytochrome *c* oxidase: proton pumping does not require Glu(I-286), Biochemistry 39 (2000) 15847–15850.
[22] P. Adelroth, M. Karpefors, G. Gilderson, F.L. Tomson, R.B. Gennis, P. Brzezinski, Proton transfer from glutamate 286 determines the transition rates between oxygen intermediates in cytochrome *c* oxidase, Biochim. Biophys. Acta 1459 (2000) 533–539.
[23] M. Svensson-Ek, J. Abramson, G. Larsson, S. Tornroth, P. Brzezinski, S. Iwata, The X-ray crystal structures of wild-type and EQ(I-286) mutant cytochrome *c* oxidases from *Rhodobacter sphaeroides*, J. Mol. Biol. 321 (2002) 329–339.
[24] H. Michel, Cytochrome *c* oxidase: catalytic cycle and mechanisms of proton pumping—a discussion, Biochemistry 38 (1997) 15129–15140.
[25] A.S. Pawate, J. Morgan, A. Namslauer, D. Mills, P. Brzezinski, S. Ferguson-Miller, R.B. Gennis, A mutation in subunit I of cytochrome oxidase from *Rhodobacter sphaeroides* results in an increase in steady-state activity but completely eliminates proton pumping, Biochemistry 41 (2002) 13417–13423.
[26] S. Yoshikawa, K. Shinzawa-Itoh, R. Nakashima, R. Yaono, E. Yamashita, N. Inoue, M. Yao, M.J. Fei, C.P. Libeu, T. Mizushima, H. Yamaguchi, T. Tomizaki, T. Tsukihara, Redox-coupled crystal structural changes in bovine heart cytochrome *c* oxidase, Science 280 (1998) 1723–1729.
[27] S. Iwata, C. Ostermeier, B. Ludwig, H. Michel, Structure at 2.8-Angstrom Resolution of Cytochrome-*C*-Oxidase from *Paracoccus denitrificans*, Nature 376 (1995) 660–669.
[28] W.R. Forsyth, J.M. Antosiewiez, A.D. Robertson, Empirical relationships between protein structure and carboxyl pK(a) values in proteins, Proteins: Struct., Funct., Genet. 48 (2002) 388–403.
[29] S. Riistama, G. Hummer, A. Puustinen, R.B. Dyer, W.H. Woodruff, M. Wikström, Bound water in the proton translocation mechanism of the haem-copper oxidases, FEBS Lett. 414 (1997) 275–280.
[30] I. Hofacker, K. Schulten, Oxygen and proton pathways in cytochrome *c* oxidase, Proteins: Stuct., Funct., Genet. 30 (1998) 100–107.
[31] R. Pomès, G. Hummer, M. Wikström, Structure and dynamics of a proton shuttle in cytochrome *c* oxidase, Biochim. Biophys. Acta 1365 (1998) 255–260.
[32] D.M. Medvedev, I. Daizadeh, A.A. Stuchebrukhov, Electron transfer tunneling pathways in bovine heart cytochrome *c* oxidase, J. Am. Chem. Soc. 122 (2000) 6571–6582.
[33] X. Zheng, D.M. Medvedev, J. Swanson, A.A. Stuchebrukhov, Computer simulation of water in cytochrome *c* oxidase, Biochim. Biophys. Acta 1557 (2003) 99–107.
[34] M. Wikström, M.I. Verkhovsky, G. Hummer, Water-gated mechanism of proton translocation by cytochrome *c* oxidase, Biochim. Biophys. Acta 1604 (2003) 61–65.
[35] A.A. Stuchebrukhov, Electron transfer reactions coupled to proton translocation: cytochrome oxidase, proton pumps, and biological energy transduction, J. Theor. Comput. Chem. 2 (2003) 91–118.
[36] R.I. Cukier, Theory and simulation of proton-coupled electron transfer, hydrogen-atom transfer, and proton translocation in proteins, Biochim. et Biophysica. Acta (in press).

[37] S. Scheiner, X. Duan, in: D.A. Smith (Ed.), Modelling the Hydrogen Bond, ACS Symposium Series, American Chemical Society, Washington, D.C, 1994, p. 125.
[38] S. Scheiner, Hydrogen Bonding: A Theoretical Perspective, Oxford Univ. Press, New York, 1997.
[39] J. Florián, S. Scheiner, Variation of atomic charges during proton transfer in hydrogen bonds, J. Comput. Chem. 15 (1994) 553–560.
[40] W.F. van Gunsteren, H.J.C. Berendsen, GROMOS Manual, University of Groningen, 1987.
[41] I.N. Levine, Quantum Chemistry, vol. I, Allyn and Bacon, Boston, 1970.
[42] M.D. Feit, J.J.A. Fleck, A. Steiger, Solution of the Schrödinger equation by a spectral method, J. Comput. Phys. 47 (1982) 412.
[43] R. Kosloff, Time-dependent quantum-mechanical methods for molecular dynamics, J. Phys. Chem. 92 (1988) 2087–2100.
[44] R.I. Cukier, S.A. Seibold, Molecular dynamics simulations of prostaglandin endoperoxide II synthase-1: role of water and the mechanism of compound I formation from hydrogen peroxide, J. Phys. Chem., B 106 (2002) 12031–12044.
[45] R.W. Hockney, J.W. Eastwood, Computer Simulation Using Particles, McGraw-Hill, New York, 1981.
[46] M.P. Allen, D.J. Tildesley, Computer Simulation of Liquids, Clarendon Press, Oxford, 1987.
[47] Coordinates kindly provided by Professor S. Ferguson-Miller.
[48] E.I. Solomon, U.M. Sundaram, T.E. Machonkin, Multicopper oxidases and oxygenases, Chem. Rev. 96 (1996) 2563–2605.
[49] M. Branden, F. Tomson, R.B. Gennis, P. Brzezinski, The entry point of the K-proton-transfer pathway in cytochrome *c* oxidase, Biochemistry 41 (2002) 10794–10798.
[50] M.J. Frisch, G.W. Trucks, H.B. Schlegel, G.E. Scuseria, M.A. Robb, J.R. Cheeseman, V.G. Zakrzewski, J.A. Montgomery, Jr., R.E. Stratmann, J.C. Burant, S. Dapprich, J.M. Millam, A.D. Daniels, K.N. Kudin, M.C. Strain, O. Farkas, J. Tomasi, V. Barone, M. Cossi, R. Cammi, B. Mennucci, C. Pomelli, C. Adamo, S. Clifford, J. Ochterski, G.A. Petersson, P.Y. Ayala, Q. Cui, K. Morokuma, P. Salvador, J.J. Dannenberg, D.K. Malick, A.D. Rabuck, K. Raghavachari, J.B. Foresman, J. Cioslowski, J.V. Ortiz, A.G. Baboul, B.B. Stefanov, G. Liu, A. Liashenko, P. Piskorz, I. Komaromi, R. Gomperts, R.L. Martin, D.J. Fox, T. Keith, M.A. Al-Laham, C.Y. Peng, A. Nanayakkara, M. Challacombe, P.M.W. Gill, B. Johnson, W. Chen, M.W. Wong, J.L. Andres, C. Gonzalez, M. Head-Gordon, E.S. Replogle, J.A. Pople. Revision A.11.1 ed., Gaussian, Pittsburgh, PA, 2001.
[51] We are indebted to Professor Y. Bu for carrying out this calculation..
[52] J.J. Dwyer, A.G. Gittis, D.A. Karp, E.E. Lattman, D.S. Spencer, W.E. Stites, B.E. Garcia-Morena, High apparent dielectric constants in the interior of a protein reflect water penetration, Biophys. J. 79 (2000) 1610–1620.
[53] A. Namslauer, A. Aagaard, A. Katsonouri, P. Brzezinski, Intramolecular proton-transfer reactions in a membrane-bound proton pump: the effect of pH on the peroxy to ferryl transition in cytochrome *c* oxidase, Biochemistry 42 (2003) 1488–1498.
[54] A.L. Lehninger, Biochemistry, Worth, New York, 1970.
[55] L. Banci, Molecular dynamics simulations of metalloproteins, Curr. Opin. Chem. Biol. 7 (2003) 143–149.
[56] T. Dudev, C. Lim, Principles governing Mg, Ca and Zn binding and selectivity in proteins, Chem. Rev. 103 (2003) 773–787.
[57] M. Karpefors, P. Ädelroth, P. Brzezinski, Localized control of proton transfer through the D-pathway in cytochrome *c* oxidase: application of the proton-inventory technique, Biochemistry 39 (2000) 6850–6856.